Electromechanical strain in Bi(Zn$_{1/2}$Ti$_{1/2}$)O$_3$–(Bi$_{1/2}$Na$_{1/2}$)TiO$_3$–(Bi$_{1/2}$K$_{1/2}$)TiO$_3$ solid solutions

Eric A. Patterson,[1] David P. Cann,[1] Jan Pokorny,[2] and Ian M. Reaney[2]

[1]*Materials Science, School of Mechanical, Industrial and Manufacturing Engineering, Oregon State University, Corvallis, Oregon 97331, USA*
[2]*Department of Materials Science and Engineering, University of Sheffield, Sheffield S1 3JD, United Kingdom*

Solid solutions ceramics of the Bi(Zn$_{0.5}$Ti$_{0.5}$)O$_3$–(Bi$_{0.5}$K$_{0.5}$)TiO$_3$–(Bi$_{0.5}$Na$_{0.5}$)TiO$_3$ ternary system for <20 mol. % BZT were created and confirmed to be single phase using x-ray diffraction. The dielectric dispersion showed decreasing T_{max} of the dielectric spectrum with a broadening of the transition with increasing BZT content. At 2.5BZT–40BKT–57.5BNT, a secondary transition commonly observed for morphotropic phase boundary (MPB) BNT–BKT was observed. The ferroelectric behavior of the system was characterized by a transition where the polarization hysteresis showed a severe pinching effect on remanent polarization (20.8 μC/cm^2 at 2.5% BZT) as BZT contents was increased (P_r = 2.3 μC/cm^2 at 20% BZT). Similarly, as the temperature increased to 175 °C, the remanent polarization of the 2.5% BZT composition significantly reduced to 2.1 μC/cm^2. The onset of this transition corresponds to the lower temperature frequency dispersion observed in the dielectric spectrum. The strain hysteresis experienced analogous transition to the polarization, with a change in shape from typical ferroelectric butterfly to a complete loss of negative strain as BZT concentration increased. Maximum strain values of 0.33% were observed at 5-40-55 accompanied by a large $d_{33}^* = 547$ pm/V. © *2012 American Institute of Physics.* [http://dx.doi.org/10.1063/1.4714346]

INTRODUCTION

Much recent research has focused on the development of Bi-based piezoelectrics as environmentally compatible alternatives to lead zirconate titanate (PZT) since the Bi^{3+}, like the Pb^{2+} ion, is highly polarizable due to a lone electron pair.[1,2] Compounds such as (Bi$_{0.5}$K$_{0.5}$)TiO$_3$ (BKT) and (Bi$_{0.5}$Na$_{0.5}$)TiO$_3$ (BNT), and their solid solutions with BaTiO$_3$ and other tetragonal perovskites exhibit usable piezoelectric properties[3–12] and are considered as candidates to replace Pb-based materials.[11,13,14] BNT has recently been shown to have a monoclinic (Cc) rather than rhombohedral (R3c) structure at room temperature, and although it shows a relatively high remanent polarization P_r = 38 μC/cm^2, such values can only be achieved at very high applied fields due to its extremely large coercive field, E_c = 73–75 kV/cm.[12,15,16] BKT is tetragonal but also requires a large field [E_{app} > 100 kV/cm] to yield its maximum polarization (P_{max} = 33 μC/cm^2) and also has an unsuitably large E_C = 52.5 kV/cm^3. Thus, effective poling of BKT and BNT ceramics is challenging with large d_{33} values difficult to obtain at low fields.

BKT–BNT is one of the closest PbO-free materials in behavior to PZT, with optimum piezoelectric performance in the vicinity of an morphotropic phase boundary (MPB) between R3c and tetragonal (P4mm) phases[17] with P_r = 38 μC/cm^2, piezoelectric coefficient, d_{33} = 167 pC/N, and electromechanical coupling coefficient, k_{33} = 0.56.[14] It has proved relatively easy to form solid solutions of BNT–BKT with other perovskites such as BaTiO$_3$ and (Bi$_{0.5}$Li$_{0.5}$)TiO$_3$ (BLT) in which an MPB may be located, examples of which may be found in Ref. 18. More recently, attention has focused on forming solid solution of BNT–BKT with end members that are unstable in ambient, such as Bi(Zn$_{1/2}$Ti$_{1/2}$)O$_3$. Huang *et al.*

first reported the structure and electrical properties of (1 − x)(Bi$_{1/2}$K$_{1/2}$)TiO$_3$–x Bi(Zn$_{1/2}$Ti$_{1/2}$)O$_3$ solid solutions (BKT–BZT) (Ref. 19) and demonstrated that BZT improved the density, dielectric, and piezoelectric properties of BK.[3,19] P_r (11.8 μC/cm^2) for BKT–BZT was not as high as in the BNT–BKT system, but the maximum strain, S_{MAX} = 0.15%, was significantly improved over that practically achieved in pure BKT.[3,6,19]

In this contribution, the ternary BNT–BKT–BZT solid solutions are explored. Starting compositions were chosen based on the reported properties of 0.1BZT–0.9BKT.[19] Ternary space was first mapped by varying the K/Na ratio, in accordance with the formula, 0.1BZT–(0.9–z)BKT–(z)BNT. Subsequently, composition space was explored by fixing BKT at 0.4 and the varying the BZT/BNT ratio according to the formula, xBZT–(0.4)BKT–(0.6–x)BNT. For convenience, all compositions are referred to by their mole percentage of X–Y–Z to indicate X%BZT–Y%BKT–Z%BNT throughout this article.

EXPERIMENTAL

Compositions in the BZT–BKT–BNT ternary system were produced via conventional solid state synthesis, using starting powders (Bi$_2$O$_3$, TiO$_2$, ZnO, NaCO$_3$, and KCO$_3$) of >99.9% purity. Six hours of high energy vibratory milling using yttrium stabilized zirconia milling media in ethanol was utilized for mixing and post-calcination grinding. Calcinations were performed in covered crucibles at 900–950 °C for 6 h followed by a second 6 h vibratory milling step.

The milled, calcined powders were mixed with 3 wt. % solution of Paraloid (PL) binder, and then uniaxially cold pressed into 12.8 mm pellets at a pressure of 150 MPa. Sintering was performed at 1050–1100 °C for 4 h. X-ray diffraction

was used for phase identification between 20 and 80° 2θ on polished sintered pellets (Bruker AXS D8 Discover).

Prior to electrical measurements, samples were polished to sub-millimeter thickness and high-temperature silver paste (Heraeus C1000) was fired on both sides in air at 650 °C for 30 min. An LCR meter (Agilent 4284A) was used to measure the dielectric properties for a wide variety of frequencies and temperatures using a high temperature measurement cell (NorECS Probostat). Hysteresis measurements were made using a sawyer-tower circuit-based Radiant Technology Premier II ferroelectric test system utilizing Vision software. Strain hysteresis measurements were taken with the same system in conjunction with an MTI Instruments 2100 Fotonic Sensor. Unpolarized Raman spectra were excited with the 514.5 nm line of an Ar laser and recorded with a Renishaw inVia micro-Raman spectrometer. The spectra were corrected to the Bose–Einstein temperature factor.

RESULTS AND DISCUSSION

All peaks in x-ray diffraction data could be indexed according to a single perovskite phase for all compositions with <20% BZT as shown in Fig. 1. All ceramics achieved typically <95% of the theoretical density at sintering temperatures below 1100 °C. All compositions in this study exhibited splitting of the {$h00$} peaks, characteristic of tetragonal symmetry but as the mole fraction of BZT increased the c/a ratio increased slightly from 1.014 at 2.5 mol. % BZT to 1.017 at 20 mol. % BZT. Similarly, for 10% BZT compositions, the c/a ratio barely decreased as the temperature increased from 1.012 at room temperature to 1.014 at 200 °C. For compositions with >20% BZT, multiple phases were observed, with the assemblage dominated by perovskite and $Bi_4Ti_3O_{12}$.

The dielectric spectra for all compositions as a function of BZT concentration at 10 kHz are shown in Fig. 2(a). The dielectric maximum (T_{max}) for each composition is indicated. The data for these BZT solid solutions look somewhat similar to those for the BNT–BKT or BNT–BT binary solid solutions, with a broad maximum located between 250 °C and 350 °C.[5,6,12] Generally, as the amount of BZT increased, T_{max}

shifted to lower temperatures. In addition, with increased BZT, the transition became increasingly diffuse, and the maximum permittivity decreased. A secondary transition could be clearly resolved for compositions with 2.5% BZT, Fig. 2(b). At higher BZT concentrations, the low temperature transition cannot be identified as the overall dielectric spectra between room temperature and T_{max} became highly dispersive. The maximum permittivity and sharpest transition peak are found for 2.5% BZT with a T_{max} = 322 °C.

In the binary BKT–BNT system, compositions with >20 mol. % BKT favor tetragonal symmetry at room temperature. In the ternary compounds in this study, based on x BZT–(0.4) BKT–(0.6–x) BNT, tetragonal distortions were clearly observed in XRD data for 2.5 mol. % BZT. In Raman data obtained on a range of BZT (Fig. 3), compositions with up to 15 mol. % BZT showed a characteristic doublet at approximately 300 cm^{-1} at room temperature typical of tetragonal symmetry, in agreement with the XRD data. With increasing BZT concentration, the lower-wavenumber peak weakens in intensity. On heating compositions with 2.5% BZT, the doublet transforms gradually into a broad single mode at approximately 320 °C in agreement with T_{max} in the
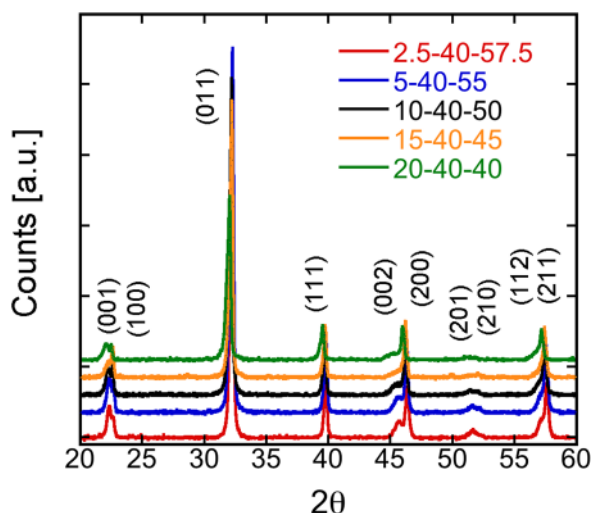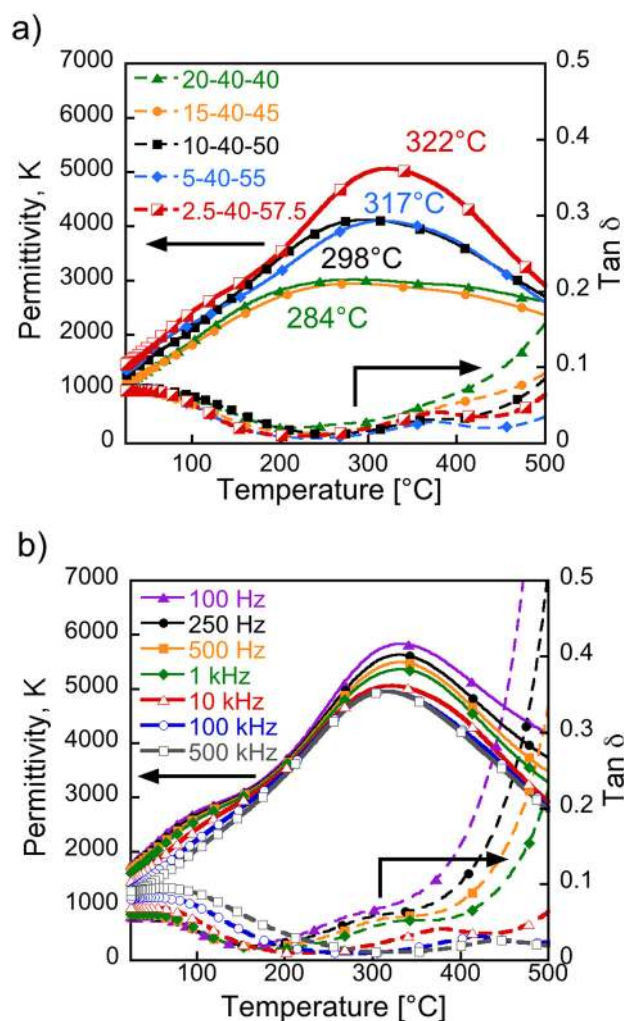

FIG. 2. (a) Dielectric properties as a function of temperature at 10 kHz for the indicated compositions (%BZT–%BKT–%BNT) and (b) frequency dispersion of the dielectric properties of the composition 2.5 BZT–40 BKT–57.5 BNT.

FIG. 1. XRD patterns as a function of 2θ for the indicated compositions (%BZT–%BKT–%BN) with peaks indexed.
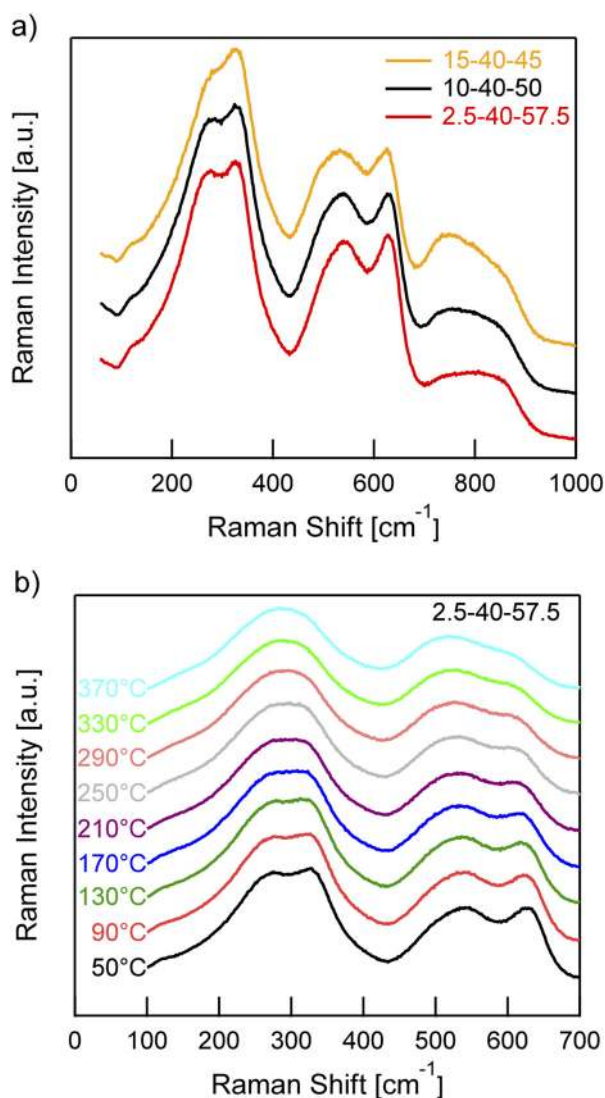
FIG. 3. Raman Spectroscopy data for (a) tetragonal 2.5%, 10%, and 15% BZT compositions at room temperature and (b) showing the tetragonal to cubic transition of 2.5–40–57.5 with increasing temperature.

dielectric data shown in Fig. 2. However, no structural anomalies were observed in the Raman or XRD data as a function of temperature that would correspond to the weak broad transition in the dielectric data at approximately 200 °C. In the binary BKT–BNT system, the broad peak in permittivity observed near 200 °C has been attributed to the emergence of either a tetragonal P4mm phase (Teranishi *et al.*) or to a pseudo-cubic phase (Hiruma *et al.*) from a rhombohedral phase at room temperature. High temperature XRD data obtained on materials in this study were largely inconclusive, however, the Raman data disagree with the interpretation of Teranishi *et al.* since the structure remains tetragonal until approximately T_{max}. The broad anomaly at 200 °C remains to be elucidated but is likely a weak non-symmetry breaking relaxation not uncommon in oxides with such complex crystal chemistry.

The polarization hysteresis behavior of the 2.5% BZT composition strongly resembled the behavior of a normal ferroelectrics with large remanent and maximum polarization values of $P_r = 20.8 \ \mu C/cm^2$ and $P_{MAX} = 30.5 \ \mu C/cm^2$,

respectively. The coercive field ($E_C = 22.0$ kV/cm) of these samples is also considerably reduced compared to the MPB compositions in the BKT–BNT binary, which are typically on the order of 40 kV/cm or larger.[20] The piezoelectric properties changed dramatically as the amount of BZT was increased to >5 mol. %, above which the remanent polarization decreased significantly. These "pinched" hysteresis loops become more severe for all subsequent compositions. At 10% BZT, the maximum polarization begins to decrease, and by 20% BZT, the loops start to exhibit pseudo-linear behavior with $P_{MAX} = 18.2 \ \mu C/cm^2$ and a negligible remanent polarization. The corresponding P–E and S–E hysteresis loops are shown in Figs. 4(a) and 4(b), respectively.

Consistent with polarization data, the electromechanical strain data also changed as a function of BZT concentration. For compositions with 2.5% BZT, the strain data exhibited a classic "butterfly" shape with approximately –0.08% negative strain, typical of domain switching for a ferroelectric. The maximum strain, $S_{MAX} = 0.22$–0.25% and corresponded to a high-field effective d_{33}^* of 408 pm/V. For 10–40–50 and
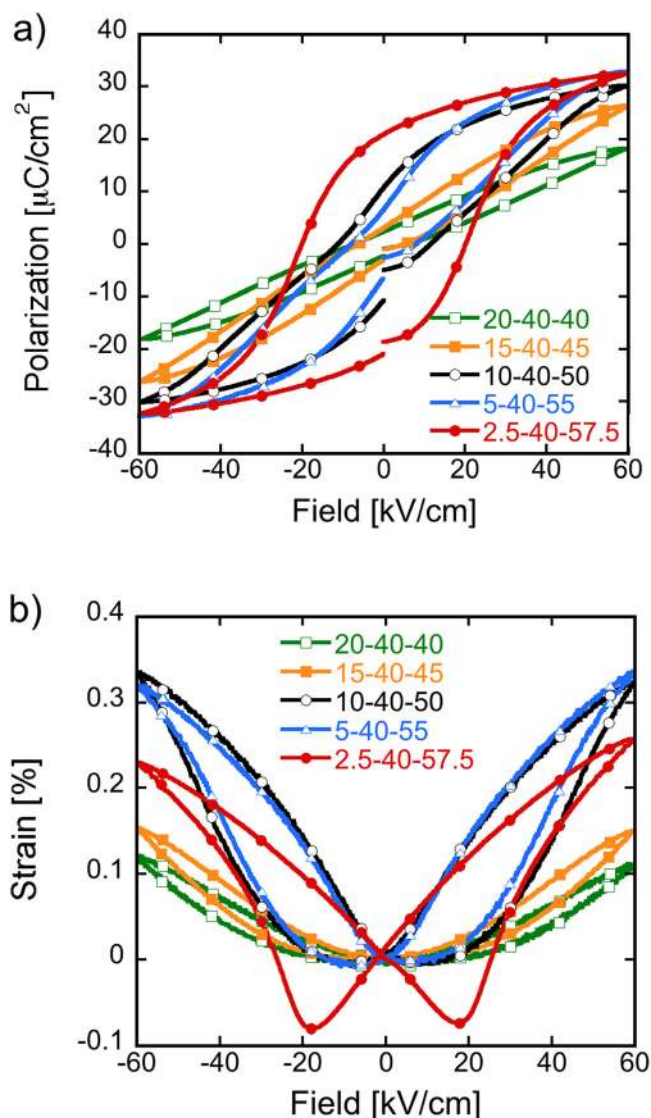

FIG. 4. (a) Polarization and (b) electromechanical strain as a function of the applied electric field for compositions with a varying amount of BZT.
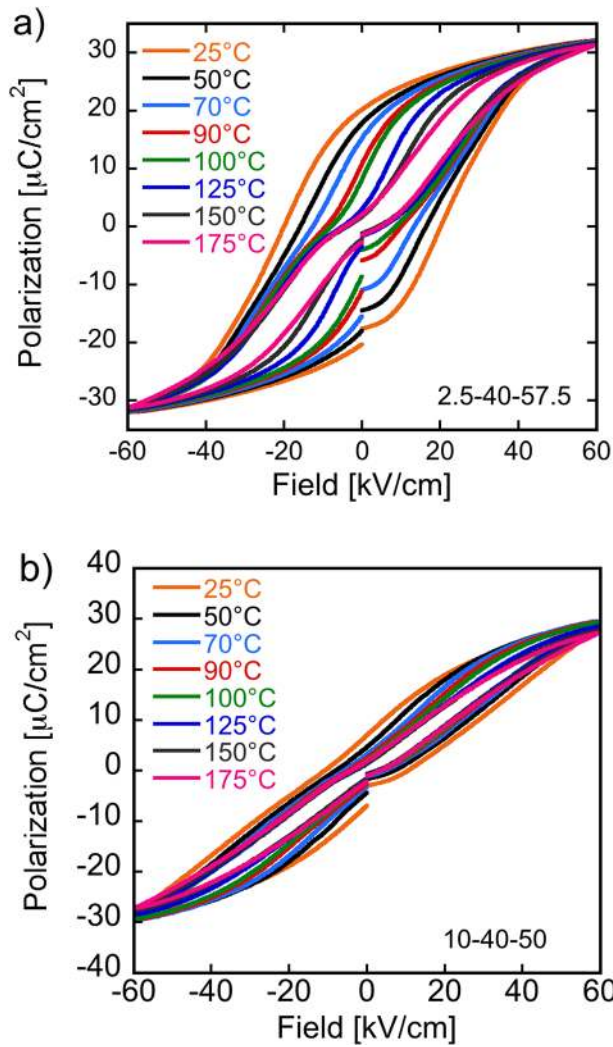
FIG. 5. Saturated polarization hysteresis as a function of temperature for (a) 2.5–40–57.5 and (b) 10–40–50 ceramics, measured at 1 Hz.

5–40–55 compositions showed $S_{MAX} \approx 0.33\%$ and were correlated with a high-field $d_{33}*$ of 547 pm/V. For all samples with >5% BZT, however, no negative strain was observed.

The electromechanical strain generally decreased in magnitude and become more parabolic and hysteretic as the concentration of BZT further increased. The strain hysteresis for the 20% BZT composition was low, with the most narrow, parabolic shape and an $S_{MAX} \approx 0.13\%$. These parabolic strain characteristics are similar to the electrostrictive behavior observed in relaxor ferroelectrics.[21]

Polarization hysteresis behavior was also investigated as a function of temperature and is shown in Fig. 5. As the temperature increased, the composition with 2.5% BZT exhibited a narrowing of the hysteresis loops, with a significant decrease in the coercive field. Above 70 °C, in addition to the decrease in coercive field, the loops became pinched, resulting in a massive reduction in remanent polarization to 2.0 $\mu C/cm^2$ at 175 °C. This pinching is similar to the effect of adding higher levels of BZT observed at room temperature. The temperature at which this pinching initiates corresponds to the onset of the frequency dispersion in the dielectric response at around 200 °C. Fig. 5(b) demonstrates a further reduction in the remanent polarization observed in the already pinched loops of the 10–40–50 composition, but the magnitude of this decrease is not as severe as in the 2.5% BZT composition.

Ternary diagrams showing S_{Max} and $d_{33}*$ for all compositions measured are displayed in Fig. 6. The maximum values in both cases are near the 10–40–50 for the 10% BZT compositions and 5–40–55 for the 40% BNT compositions. The maximum values for the high-field piezoelectric coefficient are shifted noticeably towards the BKT-rich end of the diagram compared to the location of the MPB in the binary system at 20 BKT–80 BNT. The largest S_{Max} of 0.33% values are nearly twice that of the stable binary compositions for BKT–BZT and also result from lower applied field levels.[19] The $d_{33}*$ values are nearly twice those previously reported for BNT–BKT (291 pm/V) or BNT–BT (240 pm/V) and are comparable to other high strain compositions of BNT–BT–KNN (385–560 pm/V) recently published.[11,12,17,22]

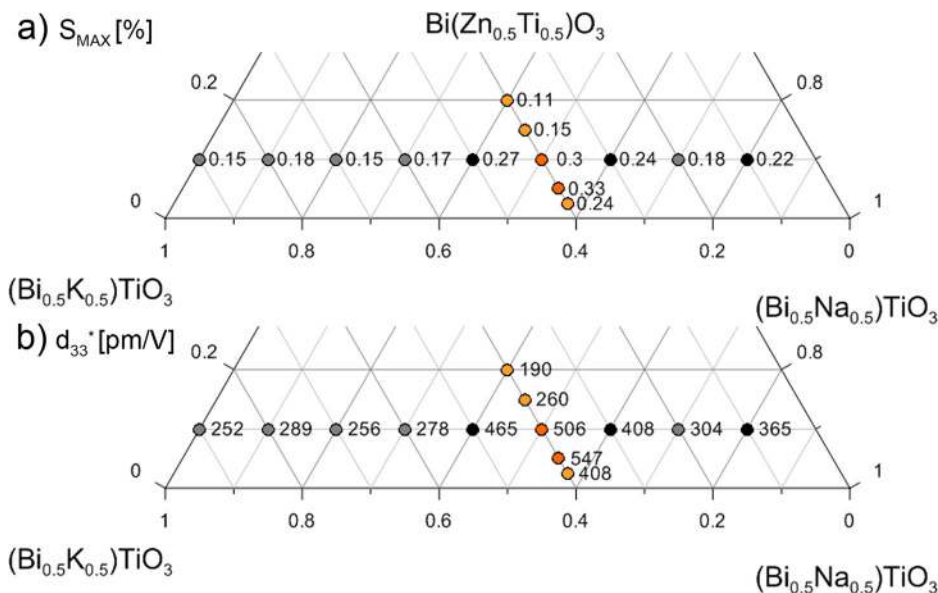The transition in hysteresis behavior is schematically illustrated in Fig. 7. The polarization hysteresis type follows

FIG. 6. (a) S_{Max} (%) and (b) $d_{33}*$ (pm/V) values plotted on the BZT–BKT–BNT phase diagram (as observed at 60 kV/cm).
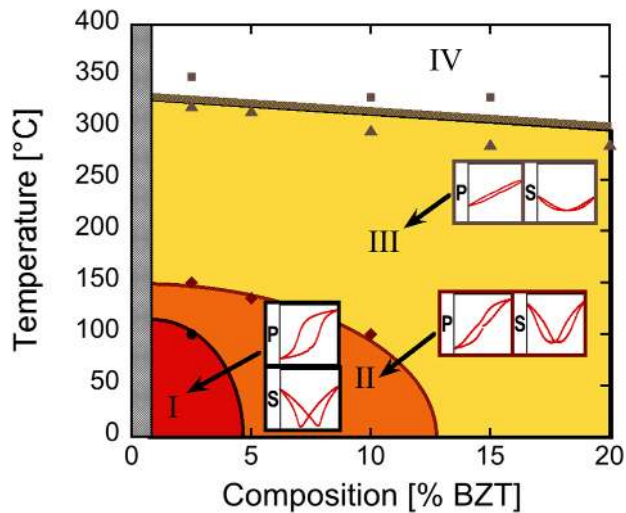
FIG. 7. Phase diagram for BZT–BNT–BKT as a function of temperature showing transition in hysteresis behaviors up to the solubility limit of 20 mol. % BZT. The circles and diamonds correspond to data taken from hysteresis measurements (● and ◆). The squares and triangles correspond to T_{max} values taken from Raman spectroscopy (■) and dielectric data (▲).

the scheme utilized by Hiruma *et al.* for similar BNT-based solid solutions. The diagram shows that fully saturated polarization hysteresis behavior dominates at low BZT concentrations and low temperatures. As the temperature increases, there is first a transition from ferroelectric to "pinched" loops with a significant reduction in remanent polarization and coercive field. This is followed by a transition to a pseudo-linear behavior at compositions above 10% BZT or temperatures above 100–150 °C up to a solubility limit of 20% BZT. Finally, above 300–350 °C compositions are paraelectric.

CONCLUSIONS

Single phase ceramics were fabricated in the BZT—BKT–BNT ternary system for <20 mol. % BZT and the dielectric and piezoelectric properties investigated. T_{max} of the dielectric spectrum steadily decreased with a corresponding broadening of the transition as BZT concentration increased. At 2.5 BZT–40 BKT–57.5 BNT, a secondary transition commonly observed for MPB BNT–BKT was observed. The polarization hysteresis showed ferroelectric behavior at 2.5% BZT with high remanent polarization of 20.8 $\mu C/cm^2$. At 20% BZT, the hysteresis of the samples becomes severely pinched, with negligible P_r (2.3 $\mu C/cm^2$). Similarly, as the temperature increased to 175 °C, the rema-

nent polarization of the 2.5% BZT composition drastically reduced to 2.1 $\mu C/cm^2$. The onset of this transition corresponds to the lower temperature frequency dispersion observed in the dielectric spectrum. The strain hysteresis also changed shape as BZT concentration increased with the typical ferroelectric butterfly gradually losing any negative strain and widening to a parabolic shape. Maximum strain values of 0.33% were observed at 5–40–55 accompanied by a large $d_{33}^* = 547$ pm/V.

[1] P. S. Baettig, C. F. Schelle, R. LeSar, U. V. Waghmare, and N. A. Spaldin, Chem. Mater. **17**, 1376–1380 (2005).
[2] M. R. Suchomel, A. M. Fogg, M. Allix, H. J. Niu, J. B. Claridge, and M. J. Rosseinsky, Chem. Mater. **18**(21), 4987–4989 (2006).
[3] Y. Hiruma, R. Aoyagi, H. Nagata, and T. Takenaka, Jpn. J. Appl. Phys. (Part 1) **44**(7A), 5040–5044 (2005).
[4] M. Nemoto, H. Nagata, Y. Hiruma, and T. Takenaka, Jpn. J. Appl. Phys. (Part 1) **47**(5), 3829–3832 (2008).
[5] R. Ranjan and A. Dviwedi, Solid State Commun. **135**(6), 394–399 (2005).
[6] S. Zhao, G. Li, A. Ding, T. Wang, and Q. Yin, J. Phys. D: Appl. Phys. **39**(10), 2277–2281 (2006).
[7] S. Zhang, T. R. Shrout, H. Nagata, Y. Hiruma, and T. Takenaka, IEEE Trans. Ultrason. Ferroelectr. Freq. Control **54**(5), 910–917 (2007).
[8] V. A. Isupov, Ferroelect. Rev. **315**, 123–147 (2005).
[9] H. Nagata, M. Yoshida, Y. Makiuchi, and T. Takenaka, Jpn. J. Appl. Phys. (Part 1) **42**(12), 7401–7403 (2003).
[10] T. Takenaka, H. Nagata, and Y. Hiruma, Jpn. J. Appl. Phys. (Part 1) **47**(5), 3787–3801 (2008).
[11] T. R. Shrout and S. J. Zhang, J. Electroceram **19**, 113–126 (2007).
[12] T. Takenaka, H. Nagata, and Y. Hiruma, IEEE Trans. Ultrason. Ferroelectr. Freq. Control **56**(8), 1595–1612 (2009).
[13] Y. Hiruma, T. Watanabe, H. Nagata, and T. Takenaka, Jpn. J. Appl. Phys. (Part 1) **47**(9), 7659–7663 (2008).
[14] Y. Hiruma, K. Yoshii, H. Nagata, and T. Takenaka, J. Appl. Phys. **103**(8), 084121 (2008).
[15] B. Jaffe, W. R. Cook, and H. Jaffe, *Piezoelectric Ceramics* (Academic, New York, 1971).
[16] E. Aksel, J. S. Forrester, J. L. Jones, P. A. Thomas, K. Page, and M. R. Suchomel, Appl. Phys. Lett. **98**(15), 152901:1–3 (2011).
[17] K. Yoshii, Y. Hiruma, H. Nagata, and T. Takenaka, Jpn. J. Appl. Phys. (Part 1) **45**(5B), 4493–4496 (2006).
[18] R. E. Eitel, C. A. Randall, T. R. Shrout, P. W. Rehrig, W. Hackenberger, and S. E. Park, Jpn. J. Appl. Phys. (Part 1) **40**(10), 5999–6002 (2001).
[19] C. C. Huang, V. Naratip, and D. P. Cann, IEEE Trans. Ultrason. Ferroelectr. Freq. Control **56**(7), 1304–1308 (2009).
[20] A. Sasaki, T. Chiba, Y. Mamiya, and E. Otsuki, Jpn. J. Appl. Phys. (Part 1) **38**, 5564 (1999).
[21] J. Kling, X. Tan, W. Jo, H.-J. Kleebe, H. Fuess, and J. Rödel, J. Am. Ceram. Soc. **93**(9), 2452–2455 (2010).
[22] S.-T. Zhang, A. B. Kounga, E. Aulbach, H. Ehrenberg, and J. Rodel, Appl. Phys. Lett. **91**(11), 112906 (2007).